Exceptional points in linear gyrokinetics

M. Kammerer, F. Merz, and F. Jenko
Max-Planck-Institut für Plasmaphysik, Boltzmannstr. 2, D-85748 Garching, Germany

(Received 6 March 2008; accepted 26 March 2008; published online 1 May 2008)

When performing linear gyrokinetic simulations, it is found that various types of microinstabilities, which are usually considered as strictly separated, can actually be transformed into each other via continuous variations of the plasma parameters. This behavior can be explained in terms of so-called exceptional points, which have their origin in the non-Hermiticity of the linear gyrokinetic operator and also occur in many other branches of physics. As a consequence, in large regions of parameter space, the designation of unstable modes should be done very carefully or even be avoided altogether. © *2008 American Institute of Physics*. [DOI: 10.1063/1.2909618]

I. INTRODUCTION

Inhomogeneous magnetized plasmas as they occur, e.g., in the context of magnetic confinement fusion, are known to exhibit a large number of "microscopic" (i.e., gyroradius-scale) instabilities driven by the background density and temperature gradients. These microinstabilities are, in turn, responsible for the turbulent transport determining the energy confinement time. They are usually described within the framework of linear gyrokinetic theory[1] which yields a first-principles based description in the low-frequency (compared to the ion gyrofrequency) domain. Now, it is commonplace to classify them according to some of their key characteristics, and to study them in some ideal limit. On the other hand, it has been known for a long time that under certain conditions, different mode types can "mix" or "merge." Nevertheless, it is usually assumed that by continuously changing some plasma parameters, one can trace back a mode to some region of parameter space in which its identity is clear without ambiguity. In the present paper, we will show, however, that this idea in general does not work. Instead, for parameter regimes where two modes are unstable simultaneously, we find that continuous parameter changes about so-called exceptional points (EPs) (Ref. 2) can connect the seemingly disconnected modes. In fact, in these cases the topological structure of both the real frequency and the linear growth rate in a two-dimensional parameter space is identical to that of a Riemann surface for the function $f(z)=\sqrt{z}$ in the complex plane, and circling the EP only once turns one microinstability into the other one, such that only after two turns, one retains the original mode. It is the goal of this work to investigate this property of the linear gyrokinetic equations, understand its origin, connect it to similar phenomena in other physics areas, e.g., quantum mechanics, and discuss its implications.

The remainder of this paper is organized as follows: In Sec. II, we will present some gyrokinetic simulation results obtained with the GENE code[3,4] in its linear eigenvalue mode of operation. In this context, we will encounter special locations in two-dimensional parameter spaces, at which both the complex frequencies *and the eigenvectors* of two unstable modes become identical. Thus, an EP differs fundamentally from the situations of usual "quantum degeneracy" in quantum mechanics, where the eigenvalues coincide, whereas the eigenvectors do not. Several such examples shall be given. In Sec. III, we will then discuss some of the basic properties of the linear gyrokinetic equations, which will help us to understand the origin of this phenomenon. In Sec. IV, we will present a more detailed discussion of EPs, including their occurrence in different branches of physics. Finally, some conclusions are drawn in Sec. V.

II. RESULTS FROM LINEAR GYROKINETICS

The simulations presented below are all performed with the gyrokinetic plasma turbulence code GENE (Res. 3 and 4) in its linear mode of operation. While it usually works as an initial value solver, GENE has recently been extended by an interface to the SLEP*c* (Ref. 5) library, a fully parallel iterative solver for eigenvalue problems. SLEP*c*, in turn, is based on the PETS*c* package.[6,7] Using this eigenvalue setup, it is possible (for a given set of plasma parameters and perpendicular wavenumbers) to compute not only the dominant microinstability (as is also possible in an initial value simulation) but also subdominant unstable modes.

For simplicity, we use the well-known $\hat{s}$-α model magnetohydrodynamic equilibrium with $\hat{s}=0.8$, $\alpha=0$, $q=1.4$, and $\epsilon_t=r/R=0.16$. We treat two particle species, electrons and (singly charged) ions, where the mass ratio is chosen to be $m_e/m_i=5.45\cdot10^{-5}$; for the binormal wavenumber, we take $k_y\rho_s=0.2$, which is where nonlinear transport spectra typically tend to peak, and the radial box size is set to $L_x=1/(k_y\rho_s\hat{s})=6.25\rho_s$. Unless stated otherwise, we choose $\beta\equiv 8\pi n_0 T_{\mathrm{ref}} B_{\mathrm{ref}}^{-2}=2\cdot10^{-4}$ and a temperature ratio of unity, $T_e/T_i=1$. The resulting eigenvalues—whose real and imaginary parts correspond, respectively, to the linear growth rates and real frequencies—are normalized with respect to c_s/R.

In the following, we will present linear gyrokinetic simulation results obtained with GENE.

First, we want to study an example with density gradients and both electron and ion temperature gradients switched on. To assure convergence also of the subdominant modes, we employ a (relatively high) numerical resolution of 11 k_x modes (corresponding to 11 poloidal turns), 20 parallel grid points, and 64×12 points in $v_\parallel$-μ (velocity) space. The ion temperature gradient is held fixed at $R/L_{T_i}=6$. The eigen-

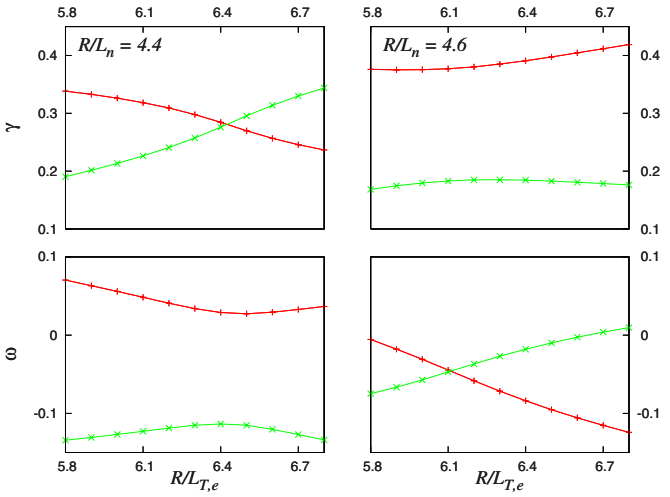

FIG. 1. (Color online) Linear growth rates γ and real frequencies ω (normalized with respect to c_s/R) as a function of R/L_{T_e} for R/L_n=4.4 (left) and R/L_n=4.6 (right).

values for two different values of R/L_n are shown in Fig. 1. For R/L_n=4.4 (left plots), the most unstable mode for low values of R/L_{T_e} exhibits a drift velocity, which points in the ion diamagnetic direction. It may therefore be identified as an ion temperature gradient (ITG) mode. Moreover, there exists a subdominant trapped electron mode (TEM) with its drift velocity pointing in the electron diamagnetic direction. Now, if R/L_{T_e} is increased to a value of about R/L_{T_e}=6.4, the TEM takes over the role of the dominant mode, i.e., one finds a crossing of the linear growth rates. This is, of course, to be expected, given that ITG modes and TEMs are, respectively, stabilized and driven by the electron temperature gradient, and mode crossings like this one have been observed frequently (see, e.g., Ref. 8). What is interesting, however, is that this picture changes *qualitatively* if we perform the same scan for a slightly larger value of the density gradient, namely for R/L_n=4.6 (see Fig. 1). Here, the two modes do not intersect in the whole R/L_{T_e} range, but it is hard to say from the frequencies whether they should be called ITG modes, TEM, "hybrid ITG/TEM modes" (see, e.g., Ref. 8) or "ubiquitous modes" (see Refs. 9–11). Obviously, at some point in the range $4.4 < R/L_n < 4.6$, a transition takes place which we want to examine in more detail now.

To this end, we vary the electron temperature gradient R/L_{T_e} and the density gradient R/L_n about their nominal values of R/L_{T_e}=6.3 and R/L_n=4.5. We compute the modes along a closed trajectory, i.e., along a square in the R/L_{T_e}-R/L_n plane around the nominal values, corresponding—as we will see—to an exceptional point. The exact path together with the results for the linear growth rates and real frequencies are displayed in Fig. 2. Of course, after one turn, the curves connect to each other again, as has to be expected. However, they connect in such a way that the roles of the dominant and subdominant mode are interchanged. Thus, through a continuous variation of plasma parameters, describing a closed path in the R/L_{T_e}-R/L_n plane, one can transform an ITG mode into a TEM. The formerly dominant mode has become the subdominant one, and vice versa. Only

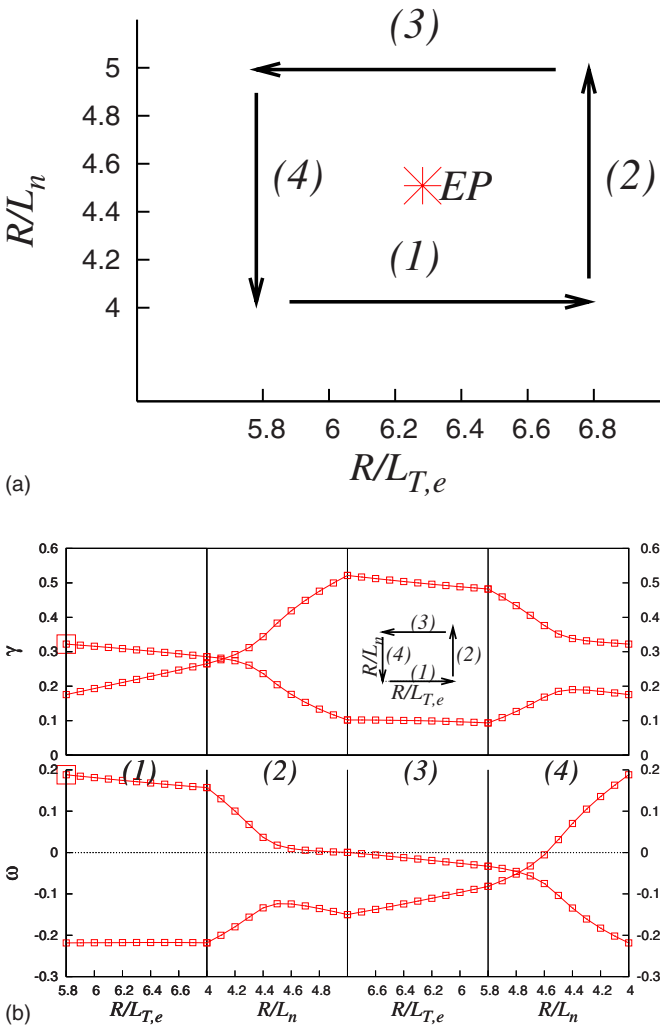

FIG. 2. (Color online) Linear growth rates γ and real frequencies ω (normalized with respect to c_s/R) for two unstable modes along a closed path in a two-dimensional parameter space spanned by R/L_{T_e} and R/L_n. The big squares denote corresponding points. After one turn, the identity of the two modes is interchanged.

after a second turn, do the curves "bite their own tails" again. As it turns out, one obtains the same scenario for any closed path around the EP in our two-dimensional parameter space, which lies sufficiently close to R/L_{T_e}=6.3 and R/L_n=4.5.

To illustrate the transformation of the two modes into each other from a somewhat different perspective, we plot their complex frequencies in Fig. 3, following the same path in parameter space as in Fig. 2. Both modes describe (only) half a turn in the complex plane during one closed turn in the parameter plane, and one closed turn in the complex plane (only) after two turns in the parameter plane. Moreover, the path in the (ω, γ) plane degenerates into a point if one decreases the area of the curve in the parameter plane, retaining the EP.

To complete the picture, the topologies of ω and γ in the R/L_{T_e}-R/L_n plane are displayed in Fig. 4, clearly showing the EP in the center. The surfaces of both the real and imaginary part of the eigenvalue are topologically equivalent to a Riemann surface for the function $f(z)=\sqrt{z}$ in the complex plane.

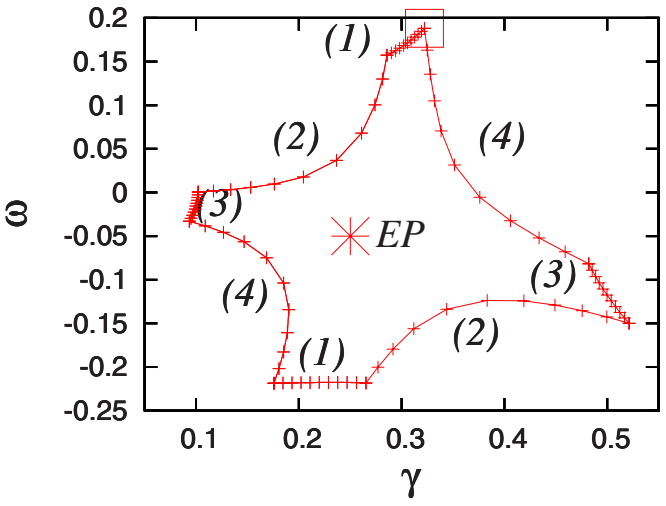

FIG. 3. (Color online) Changes of the linear growth rates γ and real frequencies ω (normalized with respect to c_s/R) along the path shown in Fig. 2. The squares in both figures correspond to each other.

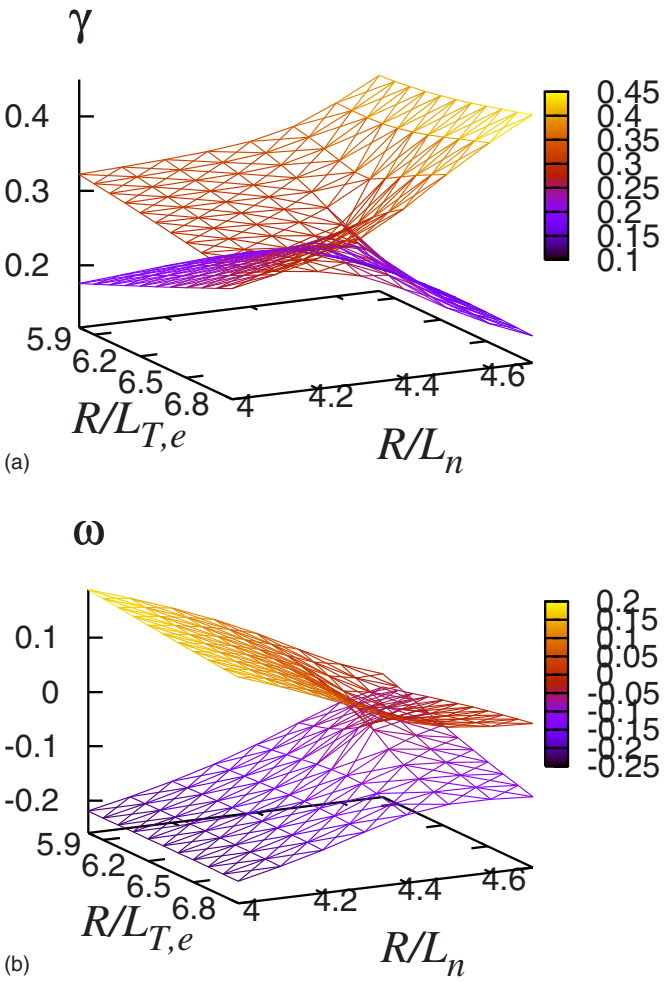

FIG. 4. (Color online) Topological structure of the linear growth rates and real frequencies of two (ITG/TEM-like) microinstabilities in R/L_{T_e}-R/L_n space, exhibiting an EP. Both structures are identical to that of a Riemann surface for the complex function $f(z)=\sqrt{z}$.

It is also interesting to investigate the behavior of the two eigenvectors in the surrounding of the EP. A respective graph is shown in Fig. 5. Here, the (absolute value of the) scalar product $p \equiv |\vec{g}_1^* \cdot \vec{g}_2|$ between the complex-valued normalized eigenvectors $\vec{g}_1$ and $\vec{g}_2$ (g represents the particles' modified distribution functions as defined in Sec. III) is displayed. This quantity can be considered as a measure of the correlation between two modes. As it turns out, p is unity at the EP, i.e., the two eigenvectors become identical. Thus, at the EP, one only has a *single* eigenvalue and a *single* eigenstate. This situation differs fundamentally from the more familiar degeneracies in (Hermitian) quantum mechanics, where two different eigenstates happen to have the same eigenvalues. We would like to point out that as one moves away from the EP, p only falls off relatively slowly, demonstrating that the two linear mode structures are still quite similar in the neighborhood of the EP. This has two interesting implications. First, computing p can be an efficient means to detect EPs. Second, given that the linear mode structure often exhibits some kind of persistence in nonlinear simulations (see, e.g., Ref. 4), the character of the resulting turbulence in the neighborhood of an EP is likely to reflect its existence. This could be true, in particular, for cases in which p remains close to unity over a relatively wide range in k_y space. One such example is shown in Fig. 6.

So far, we have studied the transition between an ITG mode and a TEM, but EPs are a pretty ubiquitous phenomenon in linear gyrokinetics as we will show in the following. For example, let us consider the question, which may be raised, e.g., in the context of Fig. 2, if a certain TEM is of the ∇T_e driven or ∇n driven type. While there are situations, in which a clear answer can be given (e.g., for $R/L_{T_e}=0$ or $R/L_n=0$), in general the situation is ambiguous. Moreover, we will demonstrate the existence of EPs for the two types of TEMs, such that one kind of mode can be turned into the other one by continuous changes of the plasma parameters. Such an EP can be found, e.g., near $R/L_n=3.1$ and $R/L_{T_e}=2$ for $R/L_{T_i}=0$ (such that ITG modes are stable) and $T_e/T_i=3$ (in line with Ref. 4). For the following simulations, we employ a numerical resolution of 7 k_x modes, 16 parallel grid points, and 64×16 points in $v_\parallel$-μ (velocity) space. In the neighborhood of these parameters, one finds two unstable modes, both drifting in the electron diamagnetic direction. In the long-wavelength regime, which we are considering, this indicates that we are dealing with two kinds of TEMs. Simi-

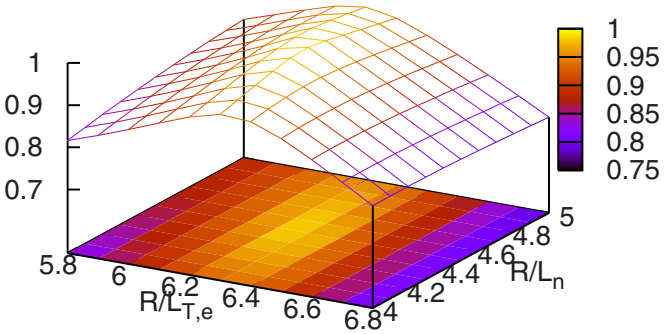

FIG. 5. (Color online) Dependence of the scalar product of two unstable TEM-like modes as a function of R/L_{T_e} and R/L_n. At the EP, one obtains unity, indicating that both modes coalesce.

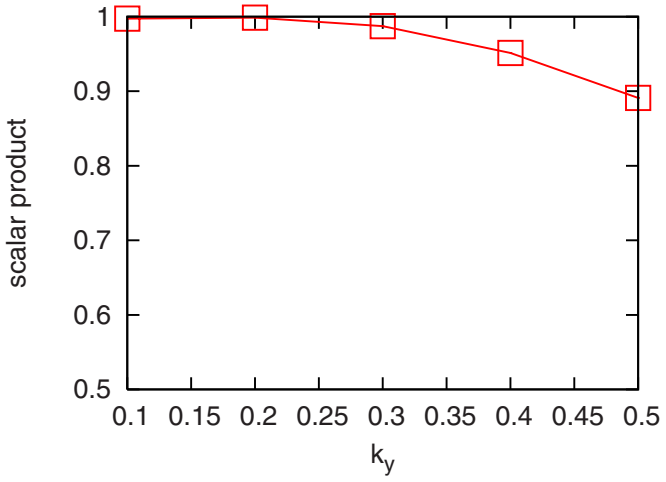

FIG. 6. (Color online) Scalar product between an ITG-like mode and a KBM-like mode as a function of the binormal wavenumber k_y (normalized to ρ_s^{-1}).

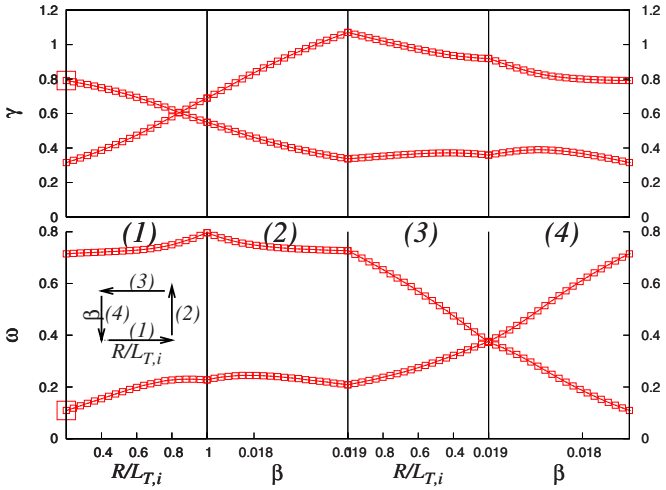

FIG. 8. (Color online) Linear growth rates γ and real frequencies ω (normalized with respect to c_s/R) for two unstable ITG/KBM-like modes along a closed path in a two-dimensional parameter space spanned by R/L_{T_i} and β.

lar to the ITG-TEM case studied before, we find that as we circle the nominal point in the R/L_n-R/L_{T_e} plane, these two modes transition into each other after one turn, making it impossible to identify both instabilities exactly (see Fig. 7).

Next, we will demonstrate that one can also find transitions between ITG modes and TEMs on the one hand, and so-called kinetic ballooning modes (KBMs) on the other hand. For this purpose, we consider the surrounding of the two points in parameter space characterized by $R/L_n=6$, $R/L_{T_i}=0.5$, $R/L_{T_e}=6$, and $\beta=0.018$ as well as by $R/L_n=6$, $R/L_{T_i}=0$, $R/L_{T_e}=5$, and $\beta=0.022$. In the first case, β and R/L_{T_i} are varied; in the second case, β and R/L_{T_e}. Here, the numerical resolution is 13 k_x modes, 32 parallel grid points, and 48×12 points in $v_\parallel$-μ (velocity) space. The results are shown in Figs. 8 and 9, exhibiting the same effects like in the cases presented above.

Finally, we demonstrate a connection between electron temperature gradient (ETG) modes, which peak in a shorter-wavelength regime, and TEMs. Here, the numerical resolution is 5 k_x modes, 16 parallel grid points, and 40×16 points in $v_\parallel$-μ (velocity) space. We employ a safety factor of $q=1.1$. Figures 10 and 11 both show the encircling of the same "exceptional line" in a three-dimensional space spanned by R/L_n, R/L_{T_e}, and k_y. In Fig. 10, it is obvious that for $R/L_{T_e}<4.65$, one can clearly distinguish between an ETG mode which is nearly stable at long wavelengths but becomes unstable at larger k_y values, and a TEM which is suppressed with increasing k_y. For $R/L_{T_e}>4.65$, the real part of the two modes are subject to repulsion, avoiding a mode crossing. This amounts to a transformation of the TEM into an ETG mode. A similar scenario in the two-dimensional parameter space spanned by R/L_n and k_y is displayed in Fig. 11.

These examples may suffice to show that EPs are rather ubiquitous in linear gyrokinetics. In fact, it is known (see

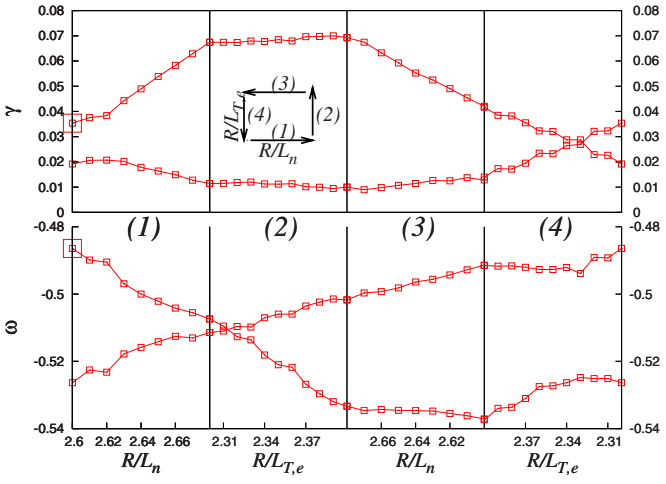

FIG. 7. (Color online) Linear growth rates γ and real frequencies ω (normalized with respect to c_s/R) for two unstable TEM-like modes along a closed path in a two-dimensional parameter space spanned by R/L_{T_e} and R/L_n.

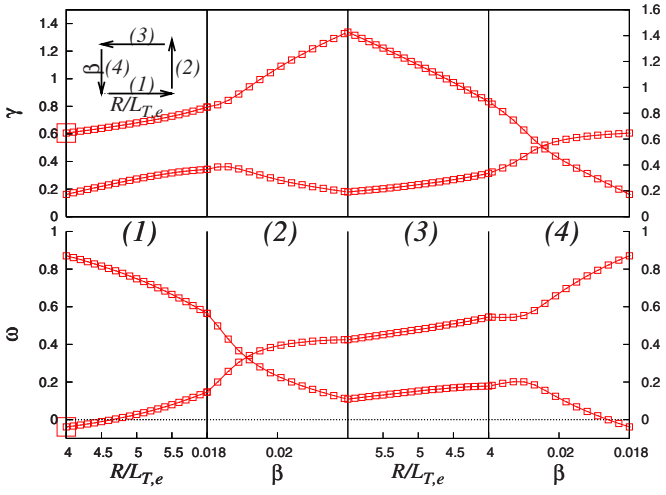

FIG. 9. (Color online) Linear growth rates γ and real frequencies ω (normalized with respect to c_s/R) for two unstable TEM/KBM-like modes along a closed path in a two-dimensional parameter space spanned by R/L_{T_e} and β.

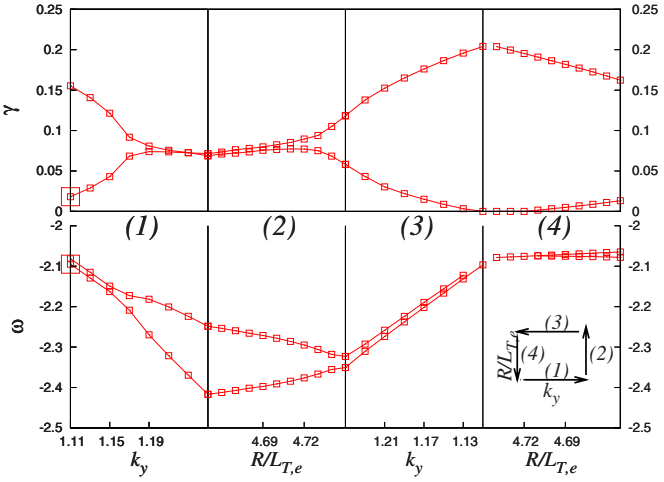

FIG. 10. (Color online) Linear growth rates γ and real frequencies ω (normalized with respect to c_s/R) for two unstable TEM/ETG-like modes along a closed path in a two-dimensional parameter space spanned by R/L_{T_e} and k_y for $R/L_n=2.2$.

Sec. IV) that EPs form $(D-2)$-dimensional structures where D is the dimensionality of the parameter space under consideration. This means that if a three-dimensional parameter space is considered, EPs are expected to form lines. This was verified by scanning along various trajectories around the EP in a three-dimensional parameter space. We expect that at least the two EPs involving the kinetic ballooning modes are connected in such a way; this conjecture is based on the fact that in the region of parameter space which connects the two EPs studied above, we were able to identify three other EPs with the same basic properties. It could actually be possible that the exceptional points studied above are somehow connected via a two-dimensional subspace in the four-dimensional space spanned by R/L_n, R/L_{T_e}, R/L_{T_i}, and β. A verification of this conjecture would require many more simulations, however, and is beyond the scope of the present work.

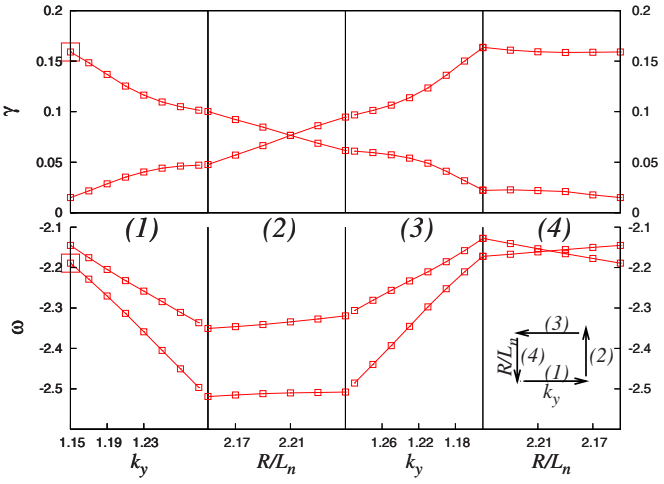

FIG. 11. (Color online) Linear growth rates γ and real frequencies ω (normalized with respect to c_s/R) for two unstable TEM/ETG-like modes along a closed path in a two-dimensional parameter space spanned by R/L_n and k_y for $R/L_{T_e}=4.65$.

III. PROPERTIES OF THE LINEAR GYROKINETIC EQUATIONS

In order to understand the phenomena described in the previous section, we now want to take a closer look at the underlying equations. The appropriate description for the very hot and dilute plasmas in the core region of present and future fusion experiments is the gyrokinetic Vlasov–Maxwell system of equations.[1] For both analytical and numerical investigations of plasma microinstabilities, the distribution function of the gyrocenters for the plasma species is usually split into a static (usually Maxwellian) background distribution function F_0, which provides the (fixed) temperature and density gradients that drive the system, and a (small) perturbation $f_j(x,y,z,v_\parallel,\mu)$, which evolves in time. This perturbation f depends on the three spatial coordinates, as well as on the parallel velocity $v_\parallel$, the magnetic moment μ, and the species label j; the dependence on the rapidly changing gyroangle has been analytically removed from the equations. Although we are using finite β values in our simulations, we first want to discuss the electrostatic version of the linearized equations in which case the modified distribution function g introduced in the previous section coincides with f. The equations for finite k_y then read

$$\frac{\partial f}{\partial t} = \mathcal{L}f = (\mathcal{L}^f + \mathcal{L}^\phi)f,$$

$$\mathcal{L}^f = -\frac{B_0\mu + 2v_\parallel^2}{\sigma B_0}\left(K_x\frac{\partial}{\partial x} + K_y\frac{\partial}{\partial y}\right) - v_T v_\parallel\frac{\partial}{\partial z} + \frac{v_T}{2}(\partial_z B_0)\mu\frac{\partial}{\partial v_\parallel},$$

$$\mathcal{L}^\phi f = -\left[\omega_{nx} + \left(v_\parallel^2 + B_0\mu - \frac{3}{2}\right)\omega_{Tx}\right]F_0\partial_y\bar{\phi} - \frac{B_0\mu + 2v_\parallel^2}{B_0}F_0(K_x\partial_x\bar{\phi} + K_y\partial_y\bar{\phi}) - v_T v_\parallel F_0\sigma\partial_z\bar{\phi},$$

$$\phi = \frac{\sum_j \pi q_j B_0\int \bar{f}_j dv_\parallel d\mu}{\sum_j \frac{q_j^2 n_{0j}}{T_{0j}}\left[1 - \Gamma_0\left(\frac{T_{0j}m_j k_\perp^2}{q_j^2 B_0^2}\right)\right]}.$$

Here, B_0 is the background magnetic field, the K's are curvature terms, q_j and v_{Tj} are the normalized charge and thermal velocities of the species, ω_n and ω_T are the radial density and temperature gradients, respectively. As a simulation domain, we use a field-aligned flux tube, where x is the radial coordinate, y is a binormal coordinate, and z is an anglelike coordinate parameterizing the direction parallel to the magnetic field. Both perpendicular coordinates are taken to be periodic (local approximation), so that a Fourier representation can be chosen for these directions. The bars, which

indicate gyroaveraging, then correspond to a simple multiplication with J_0 functions. Finite Debye length effects can be (and are) neglected in this paper.

Physically, the f_j are five-dimensional distribution functions of the various species gyrocenter coordinates, but after discretization of the spatial and velocity space dimensions, the difference between coordinates and the species label vanishes and f can be interpreted mathematically as the (finite-dimensional) state vector of the system whose time evolution is governed by the (matrix) operator $\mathcal{L}$, analogous to the Schrödinger equation in quantum mechanics. The eigenspectrum of the linear operator completely determines the linear physics; after solving the eigenvalue equation,

$$\mathcal{L}f_n = \omega_n f_n$$

(n is the index of the eigenvalue/eigenvector), the corresponding solution of the time evolution equation is trivial:

$$f_n(t) = A_0 f_n \exp(\omega_n t).$$

We now want to discuss the properties of $\mathcal{L}$, focusing first on the operator $\mathcal{L}^f$. This part of $\mathcal{L}$ is a differential operator which is block diagonal in the species label, i.e., the different species are completely decoupled. $\mathcal{L}^f$ is anti-Hermitian, which means that all eigenvalues are purely imaginary and the eigenvectors are orthogonal. The anti-Hermiticity, which is obvious from the analytical expression for the operator, is retained in the numerical scheme if the differential operators are expressed by appropriate numerical approximations and if appropriate boundary conditions are chosen. In GENE, the x and y directions are treated spectrally, whereas z and $v_\parallel$ are treated via centered finite differencing schemes; both of these schemes satisfy the above requirements. Note that numerical damping (introduced explicitly for numerical reasons or implicitly, e.g., via upwind schemes) destroys the anti-Hermiticity of $\mathcal{L}^f$.

The field part $\mathcal{L}^\phi$ is much more complicated, with its matrix representation being dense in the velocity and species coordinates (in contrast to the sparse matrix representation of the differential operators). $\mathcal{L}^\phi$ can be expressed as a matrix multiplication of a differential operator (with similar properties as $\mathcal{L}^f$) with the field operator. This combination is not (anti-)Hermitian, so that due to these terms, the eigenvalues of $\mathcal{L}$ are, in general, not purely imaginary and the eigenvectors are not orthogonal. $\mathcal{L}^\phi$ is thus the origin of the wealth of interesting phenomena occurring in linear gyrokinetics, including Landau damping, the various microinstabilities and the EPs considered in this paper.

Note that $\mathcal{L}^\phi$ couples f to the background distribution function F_0 via the electrostatic field; all of the respective terms originate from the *nonlinear* part of the Vlasov equation for the *full* distribution function $f+F_0$; they have only become part of the linear operator because of the δf splitting. Without this coupling (or alternatively without δf splitting), $\mathcal{L}^\phi$ would be zero, $\mathcal{L}$ anti-Hermitian and all modes would be neutrally stable.

Extending the above gyrokinetic equations to finite β (see, e.g., Ref. 4), f is to be replaced by the modified distribution function

$$g_j = f_j + \frac{2q_j}{m_j v_{Tj}} v_\parallel F_0 \bar{A}_{1\parallel},$$

and a few extra terms are to be added to $\mathcal{L}^\phi$, but this does not alter the arguments given above. We thus have identified two sources of non-Hermiticity in the equations: explicit or implicit numerical damping as well as the coupling to the background F_0 via the fields. We have checked that the damping, which would be a purely numerical effect in this case, is not the cause for the nontrivial structures described in the last section, the crucial source of non-Hermiticity is indeed the (physical) $\mathcal{L}^\phi$.

In contrast to (anti-)Hermitian operators, the mathematical properties of non- and pseudo-Hermitian operators are still under investigation. Recent years have seen a boost of interest for these operators, mainly in the quantum physics community, but with side effects in many other areas of physics. One very intriguing property of these operators is, as we will discuss in more detail in the next section, the existence of EPs.

IV. EXCEPTIONAL POINTS

Experimentally, EPs have been observed in crystals of light,[12] propagation of light in dissipative media,[13] microwave billiards,[14–16] ionization of atoms by lasers,[17] and electronic circuits.[18] They have been found in many areas of physics where non-Hermitian operators play a role, including quantum mechanics (for an overview, see Ref. 19). EPs have also been found in plasma physics before, namely, in the framework of a magnetohydrodynamic dynamo model[20] and also in the context of linear microinstabilities.[21] However, in the latter study, the existence of a "branch point" was only mentioned in passing, and the physics model was incomplete since several kinetic effects such as trapped particles and Landau resonances were neglected. Since EPs may not be familiar to the reader, we will give a short summary of some of their key properties.

The concept of "exceptional points" (sometimes, the expression "non-Hermitian degeneracy" is used instead) was first introduced by Kato.[2] Considering the matrix (in Jordan form) representing the non-Hermitian operator, the appearance of an EP corresponds to the formation of a nontrivial Jordan block out of a diagonal part. This means, that besides the degenerate eigenvalues, (at least) two eigenvectors of the matrix become degenerate and form a Jordan chain. These degeneracies are of co-dimension 2, which means, that in a two-dimensional parameter space, they appear as points, while they are represented as lines when the parameter space is extended to a third parameter. While we only found two eigenvectors merging in an EP at a time, it is in principle possible to have $M>2$ eigenvectors merge, which would increase the number of orbits around the EP necessary to return to the initial mode to M. In this case, for each turn, there is a cyclic "exchange" of the eigenmodes.

Degeneracies can also arise in the more familiar real symmetric or complex Hermitian cases, but with different properties.[22] In the real symmetric case, the degeneracies are also of co-dimension two, but the eigenvalue surfaces form a

double cone instead of the branch-point structure seen in Fig. 4 and are therefore also called "diabolical points." Degeneracies of complex Hermitian operators, on the other hand, have co-dimension 3.

For a more detailed discussion of EPs, see, e.g., Refs. 22 and 23.

V. CONCLUSIONS

In numerical simulations with the gyrokinetic GENE code, we found that various types of microinstabilities (like density and temperature gradient driven trapped electron modes, ITG modes, ETG modes, and kinetic ballooning modes) can be transformed into each other via continuous variations of the plasma parameters. This is caused by the nontrivial topology of the eigenvalue surfaces in regions of parameter space where two microinstabilities coexist.

As it turns out, the nontrivial topology is due to the existence of so-called exceptional points and therefore linked to the non-Hermiticity of the linear gyrokinetic operator. We have analyzed the gyrokinetic equations, discussed the sources for the non-Hermiticity of the linear operator, and given a short summary of the properties of EPs, which also occur in many other branches of physics.

These findings explain why in some parameter scans, which are usually only one-dimensional cuts through the high-dimensional parameter space, dominant and subdominant modes can be distinguished clearly, while in others they hybridize, or important properties like the drift direction change. Thus, while it is surely still useful to label the modes in the usual way in parameter ranges where the distinction is clear, a strict discrimination is not possible. This becomes very obvious close to EPs, where even a slight change of the direction of the scan axis can lead to a completely different picture, and sometimes even to a reversal of the labelling. In these cases, trying to designate the modes in the usual sense might be more confusing than helpful and should maybe be avoided altogether.

ACKNOWLEDGMENTS

We would like to thank Jose E. Roman, Matthew Knepley, and David Coster for help with the SLEP*c* and PETS*c* libraries. The simulations were performed at the Garching Computing Center.

[1] A. Brizard and T. Hahm, Rev. Mod. Phys. **79**, 421 (2007).
[2] T. Kato, *Perturbation Theory of Linear Operators* (Springer, Berlin, 1966), p. 64.
[3] F. Jenko, W. Dorland, M. Kotschenreuther, and B. N. Rogers, Phys. Plasmas **7**, 1904 (2000).
[4] T. Dannert and F. Jenko, Phys. Plasmas **12**, 072309 (2005).
[5] V. Hernandez, J. Roman, and V. Vidal, ACM Trans. Math. Softw. **31**, 351 (2005).
[6] S. Balay, K. Buschelman, V. Eijkhout, W. D. Gropp, D. Kaushik, M. G. Knepley, L. Curfman McInnes, B. F. Smith, and H. Zhang, PETSc users manual, Technical Report No. ANL-95/11, Revision 2.1.5, Argonne National Laboratory, 2004.
[7] S. Balay, K. Buschelman, W. D. Gropp, D. Kaushik, M. G. Knepley, L. Curfman McInnes, B. F. Smith, and H. Zhang, PETSc Web page, 2001, http://www.mcs.anl.gov/petsc.
[8] G. Rewoldt, R. V. Budny, and W. M. Tang, Phys. Plasmas **12**, 042506 (2005).
[9] G. Rewoldt and W. M. Tang, Phys. Fluids B **2**, 318 (1990).
[10] B. Coppi and F. Pegoraro, Nucl. Fusion **17**, 969 (1977).
[11] B. Coppi and G. Rewoldt, Phys. Rev. Lett. **33**, 1329 (1974).
[12] M. K. Oberthaler, R. Abfalterer, S. Bernet, J. Schmiedmayer, and A. Zeilinger, Phys. Rev. Lett. **77**, 4980 (1996).
[13] M. V. Berry and M. R. Dennis, Proc. R. Soc. London, Ser. A **459**, 1261 (2003).
[14] C. Dembowski, B. Dietz, H.-D. Gräf, H. L. Harney, A. Heine, W. D. Heiss, and A. Richter, Phys. Rev. Lett. **90**, 034101 (2003).
[15] C. Dembowski, B. Dietz, H.-D. Graf, H. L. Harney, A. Heine, W. D. Heiss, and A. Richter, Phys. Rev. E **69**, 056216 (2004).
[16] C. Dembowski, H.-D. Gräf, H. L. Harney, A. Heine, W. D. Heiss, H. Rehfeld, and A. Richter, Phys. Rev. Lett. **86**, 787 (2001).
[17] O. Latinne, N. J. Kylstra, M. Dorr, J. Purvis, M. Terao-Dunseath, C. J. Joachain, P. G. Burke, and C. J. Noble, Phys. Rev. Lett. **74**, 46 (1995).
[18] T. Stehmann and H. M. von Bergmann, Proc. SPIE **5777**, 495 (2005).
[19] U. Günther, I. Rotter, and B. F. Samsonov, J. Phys. A **40**, 8815 (2007).
[20] F. Stefani and G. Gerbeth, Phys. Rev. Lett. **94**, 184506 (2005).
[21] C. Z. Cheng, Phys. Fluids **25**, 1020 (1982).
[22] M. V. Berry, Czech. J. Phys. **54**, 1039 (2004).
[23] W. D. Heiss, J. Phys. A **37**, 2455 (2004).